Paired high-throughput, in situ imaging and high-throughput sequencing illuminate acantharian abundance and vertical distribution

Margaret Mars Brisbin [1]*, **Otis Davey Brunner**,[1] **Mary Matilda Grossmann**,[1,a] **Satoshi Mitarai**[1]
[1]Okinawa Institute of Science and Technology Graduate University, Onna-son, Japan

Abstract

Acantharians (supergroup Rhizaria) can be important contributors to surface primary production and to carbon flux to the deep sea, but are often underestimated because their delicate structures are destroyed by plankton nets or dissolved by chemical fixatives. As they are also uncultured, relatively little is known about acantharian biology, especially regarding their life cycles. Here, we take a paired approach, bringing together high-throughput, in situ imaging and metabarcode sequencing, to investigate acantharian abundance, vertical distribution, and life history in the western North Pacific. Concentrations of imaged acantharian cells correlated well with relative abundances of 18S rRNA gene sequences from acantharians with known, recognizable morphologies, but not to sequences corresponding to acantharians with unknown morphology. These results suggest that morphologically undescribed clades may lack the characteristic star-shaped acantharian skeleton or are much smaller than described acantharians. The smaller size of acantharians imaged at depth supports current hypotheses regarding nonsymbiotic acantharian life cycles: cysts or vegetative cells release reproductive swarmer cells in deep water and juvenile cells grow as they ascend toward the surface. Moreover, sequencing data present the possibility that some photosymbiotic acantharians may also reproduce at depth, like their nonsymbiotic, encysting relatives, which is counter to previous hypotheses. Finally, in situ imaging captured a new acantharian behavior that may be a previously undescribed predation strategy.

Acantharians are a type of radiolarian—unicellular microbial eukaryotes belonging to the phylum Retaria and supergroup Rhizaria. Acantharians in the orders Arthracanthida and Symphyacanthida (molecular clades E and F), which include the majority of described acantharian species (Decelle et al. 2012*a*), host algal endosymbionts from the haptophyte genus *Phaeocystis* (Decelle et al. 2012*b*; Mars Brisbin et al. 2018). These photosymbiotic acantharians can contribute substantially to primary production in surface waters, particularly in low-nutrient regions (Michaels 1991; Michaels et al. 1995; Decelle et al. 2013). The acantharian skeleton is composed of strontium sulfate (celestite), the densest known biomineral, which causes

Additional Supporting Information may be found in the online version of this article.

[a]Present address: Independent Scientist, O-4345 Omi-muri, Higashi-Chikuma-Gun, Nagano, Japan

acantharians to sink quickly after death (Decelle et al. 2013) and contributes to their high flux from the photic zone to the deep sea (Bernstein et al. 1987; Martin et al. 2010; Belcher et al. 2018). The biogeochemical significance of acantharians has been historically underestimated, however, because traditional methodologies undersample acantharians; plankton nets destroy delicate acantharian cell structures (Michaels 1988) and common chemical fixatives (e.g., formaldehyde) dissolve acantharian skeletons (Beers and Stewart 1970). Environmental sequencing surveys have revealed that acantharians account for large numbers of ribosomal RNA gene sequences in metabarcode and clone library data sets from the water column and sediment traps in diverse ecosystems, including tropical and subtropical regions (Fontanez et al. 2015; Hu et al. 2018), polar regions (Martin et al. 2010; Decelle et al. 2013), and productive temperate coastal regions (Countway et al. 2010; Gutierrez-Rodriguez et al. 2019). However, the relationship between sequence abundance and acantharian biomass or flux is not clear and is complicated by acantharians being multinucleated and having multiple life stages, including encystment and reproductive swarmer production (Decelle and Not 2015).

DNA metabarcoding—sequencing a region of the small-subunit ribosomal RNA gene for an entire community—has been extensively applied to estimating microbial community structure (e.g., de Vargas et al. 2015; Pernice et al. 2016).

While this method has undoubtedly revolutionized our understanding of microbial diversity in different ecosystems, it has several significant limitations. First, metabarcoding and other meta'omics produce compositional data, meaning that the abundance estimated for any single group is inherently influenced by the abundance of other groups (Gloor et al. 2017). This issue is further complicated by the varying nucleus and gene-copy numbers among protists (Gong and Marchetti 2019), including among radiolarians (Decelle et al. 2014; Biard et al. 2017). Additionally, while radiolarians have a single numerically dominant ribosomal RNA gene sequence, there can be some intraindividual sequence variation (Decelle et al. 2014). Variable gene-copy and nucleus number is especially problematic because it precludes the possibility of extrapolating absolute abundances from sequence counts and cell counts—if the cell abundance to sequence abundance ratio was consistent, absolute abundance of a group could be determined by multiplying the relative sequence abundance of that group with the total cell count (Gong and Marchetti 2019). The second major limitation of DNA metabarcoding is that DNA can persist after a cell dies and, therefore, does not reflect metabolic state. As a result, it is unknowable whether DNA sequences derive from actively metabolizing cells, dormant cells or cysts, reproductive cells, or dead cells and detritus (Torti et al. 2015). This is particularly relevant in evaluating acantharian abundances and relative contributions to biogeochemical cycles since acantharian vegetative cells, reproductive cells, and cysts will differentially contribute to photosynthesis, grazing/predation, and carbon flux (Decelle et al. 2013).

While not yet as widely adopted as molecular methods, high-throughput, in situ imaging systems are being used to quantitatively assess abundances of marine microbes and other components of the plankton (Dennett et al. 2002; Grossmann et al. 2015; Biard et al. 2016). Such imaging systems can drastically improve the spatial resolution of sampling and process much larger volumes of water than are included in DNA surveys. Furthermore, imaging cells where they naturally occur and in their native orientation can reveal previously undescribed behaviors and associations (Greer et al. 2013; Peacock et al. 2014; Gaskell et al. 2019). Analyzing data from high-throughput imaging, however, is still challenging; processing images and creating training sets for use with machine learning algorithms requires expertise in plankton taxonomy and is time-intensive (Orenstein et al. 2015). The taxonomic resolution attainable with a particular imaging system depends on image size and quality—with an important trade-off between resolution and sampling volume—but will almost always be less than is attainable with molecular methods. Furthermore, taxonomic resolution will vary for different taxonomic groups and will be higher for those with more defined morphological features and lower for organisms, like flagellates, that lack identifying features (Sieracki et al. 2010). Finally, a single imaging system cannot image the entire size-range of marine plankton, necessitating multiple

systems to holistically characterize plankton communities, but combining data from different systems can also be challenging, in part, because different instruments have widely ranging sampling volumes (Lombard et al. 2019). Vegetative acantharian cells, with their characteristic star-shaped skeletons, are particularly amenable to imaging surveys (Biard et al. 2016), but distinguishing acantharian reproductive cells or cysts with high-throughput, in situ imaging may not be possible.

DNA metabarcoding and high-throughput in situ imaging both have benefits and drawbacks as methods for assessing plankton abundance and community structure. By applying these methods together, we aim to better characterize acantharian abundance, water-column distribution, and life history. In this study, we deployed the BellaMare In Situ Ichthyoplankton Imaging System (ISIIS) small-imager/area-scanner (Cowen and Guigand 2008; www.planktonimaging.com/smaller-imagers) at four sites along the Ryukyu Archipelago in the western North Pacific. We additionally collected replicate water samples for DNA sequencing from the surface, subsurface chlorophyll maximum (SCM), middle water column, and about 10 m above the seafloor from each site where imaging was performed and 10 additional sites along the Ryukyu Archipelago. Water samples were sequentially size fractionated in an effort to separate acantharian vegetative cells from reproductive swarmers. We compare the relative abundance of acantharian sequences in the larger size fraction with cell counts from imaging profiles to assess the relationship between acantharian relative sequence abundance and
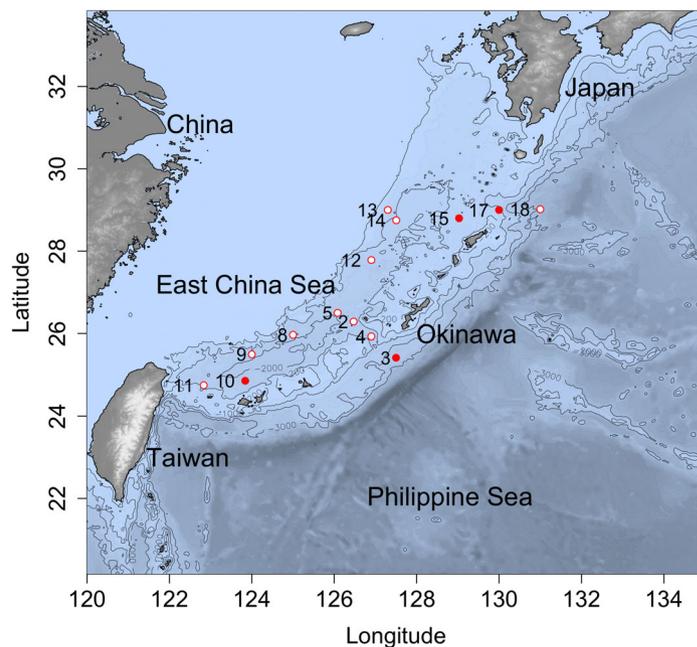

Fig. 1. Map of sampling station locations in the western North Pacific. Stations where water samples for DNA analysis were collected and high-throughput imaging was also performed are marked with closed red circles. Stations where only water samples for DNA analysis were collected are marked with open red circles.

imaged cell abundance. Metabarcoding results are further analyzed to evaluate the taxonomic distribution of acantharians by depth in the western North Pacific and we consider results from size fractionation in the context of hypothesized acantharian life cycles.

Methods

Sampling locations

Water samples for DNA sequencing were collected from 14 sites spanning the length of the Ryukyu Archipelago during the Japan Agency for Marine-Earth Science and Technology (JAMSTEC) MR17-03C cruise from 29 May 2017 to 13 June 2017 (Fig. 1). The JAMSTEC DEEP TOW 6KCTD system, a towable frame outfitted with several imaging systems and a conductivity-temperature-depth (CTD) sensor, was additionally deployed at four of the sampling sites (3, 10, 15, and 17), to take vertical profiles of plankton images, to a maximum depth of 1000 m (Supporting Information Fig. S1A).

Image acquisition and processing

An ISIIS small imager/area-scanner (BellaMare, San Diego, California) was attached to the DEEP TOW (Supporting Information Fig. S1) and set up to image organisms greater than 250 μm in diameter and smaller than the imaging area of the camera (approximately 25 cm^2). The ISIIS camera was programmed to take one photo per second, coinciding with an LED flash. Each photograph imaged 0.39 L (Sta. 3 and 10) or 0.35 L (Sta. 15 and 17) parcels of water in 2448 × 2050-pixel resolution, with each pixel being 22.5 by 22.5 μm. Because the ISIIS camera was attached to the back of the DEEP TOW, only photographs taken during down-casts were considered in this study, as the forward motion of the DEEP TOW during up-casts could interfere with plankton moving naturally through the imaging area of the camera. A total of 4010 photographs were taken during the down-cast at Sta. 3, 3639 at Sta. 10, 3056 at

Sta. 15, and 2453 at Sta. 17, so that 13,158 photographs were included in the study—an equivalent of 4932 L of seawater. Down-cast photographs were manually viewed by a single researcher and regions of interest (ROIs) containing characteristically star-shaped acantharian vegetative cells were cropped and saved. The ISIIS internal clock was calibrated to match that of a Sea-Bird SBE 9 CTD (Sea-Bird Scientific, Bellevue, Washington) mounted to the DEEP TOW so that CTD data could be used to determine the depth at which each image was taken. Concentrations of imaged acantharian cells per liter were determined by normalizing acantharian cell counts to the total number of photographs taken for 10 m bins before the relationship between cell concentration and depth was evaluated. ROI image area was used as a proxy for cell size, allowing for evaluation of the relationships between mean cell size and range with depth. Figure 2 illustrates the morphological diversity and size range of acantharians imaged in this study. Acantharian ROIs and all raw images included in the study are archived on Zenodo (https://doi.org/10.5281/zenodo.3605400).

Water sampling and DNA extraction

A Niskin bottle rosette with 30 bottles (10 L) and fitted with a CTD probe (SBE 911plus, Sea-Bird Scientific) was deployed at each cruise station to collect water from the SCM (50–100 m), the middle water column (mid, 700–1500 m), and approximately 10 m above the seafloor (bottom, 776–2957 m) (Fig. 1, Supporting Information Table S1). Surface seawater was collected by bucket alongside the research vessel. Two replicates of 4.5 L (surface) from separate bucket casts or 5 L from separate Niskin bottles (SCM, mid, bottom) were sequentially filtered under gentle vacuum through 10.0-μm and 0.2-μm pore-size polytetrafluoroethylene (PTFE) filters (Millipore, Burlington, Massachusetts). Sequential size filtering was implemented in order to separate vegetative acantharian cells and cysts from reproductive swarmer cells (< 5 μm; Decelle et al. 2012*b*),
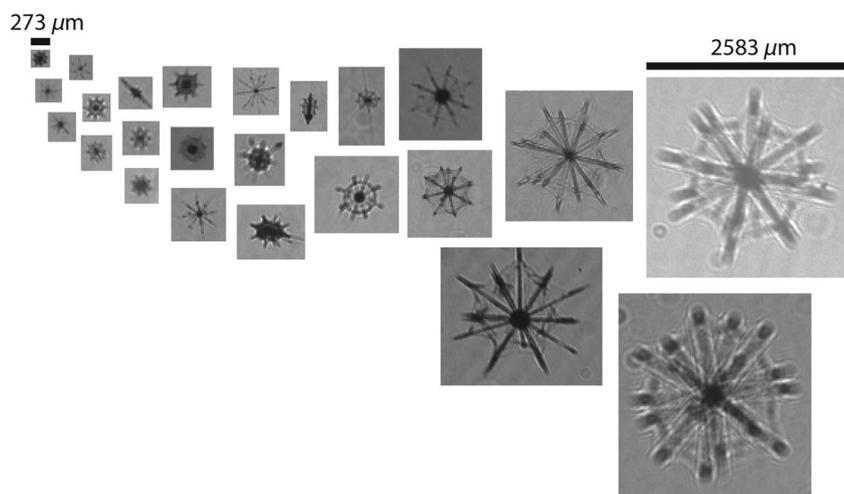

273 μm

2583 μm

Fig. 2. Acantharians imaged in this study, illustrating the morphological diversity and size range of imaged cells.

although complete separation is probably not possible. Filters were flash-frozen in liquid nitrogen and stored at −80°C.

DNA was extracted from PTFE filters (n = 224, two replicates of two filter pore sizes at four depths from 14 stations) following manufacturer's protocols for the DNeasy PowerWater Kit (Qiagen, Hilden, Germany) including the optional heating step for 10 min at 65°C to fully lyse cells. Sequencing libraries were prepared following the Illumina 16S Metagenomic Sequencing Library Preparation manual, but with universal eukaryotic primers for the V4 region of the eukaryotic 18S rRNA gene (F: CCAGCASCYGCGGTAATTCC; Stoeck et al. 2010; R: ACTTTCGTTCTTGATYR; Mars Brisbin et al. 2018) and a 58°C annealing temperature in the initial polymerase chain reaction. Amplicon libraries were sequenced by the Okinawa Institute of Science and Technology (OIST) DNA Sequencing Section on the Illumina MiSeq platform with 2 × 300-bp v3 chemistry. Amplification and sequencing were successful for 211 samples, including at least one replicate for each sample type.

Sequence analysis

Sequence data from each of four flow-cells were denoised separately using the Divisive Amplicon Denoising Algorithm (Callahan et al. 2016) through the DADA2 plug-in for QIIME 2 (Bolyen et al. 2019). Denoised amplicon sequence variant (ASV) tables were merged before taxonomy was assigned to ASVs with a naive Bayes classifier trained on the Protist Ribosomal Reference (PR^2) database (v4.11; Guillou et al. 2013) using the QIIME 2 feature-classifier plug-in (Bokulich et al. 2018). Results were imported into the R statistical environment (R Core Team 2018) for further processing with the Bioconductor package phyloseq (McMurdie and Holmes 2013). Aitchison distances, which combine centered-log-ratio normalization with Euclidean distance to reduce compositional data bias inherent in metabarcoding data, were computed with the R package CoDaSeq and were used to analyze beta diversity between different sample types (Gloor et al. 2017). Full protist communities (including all eukaryotic ASVs, except those classified as Metazoa) were analyzed first to evaluate if overall protist community composition varied by sampling depth or by filter pore size at each depth. Sequences classified as Acantharea were further analyzed separately to determine (1) if patterns by depth and filter pore size for acantharians reflected overall protist community patterns, (2) how much acantharian sequences contributed to
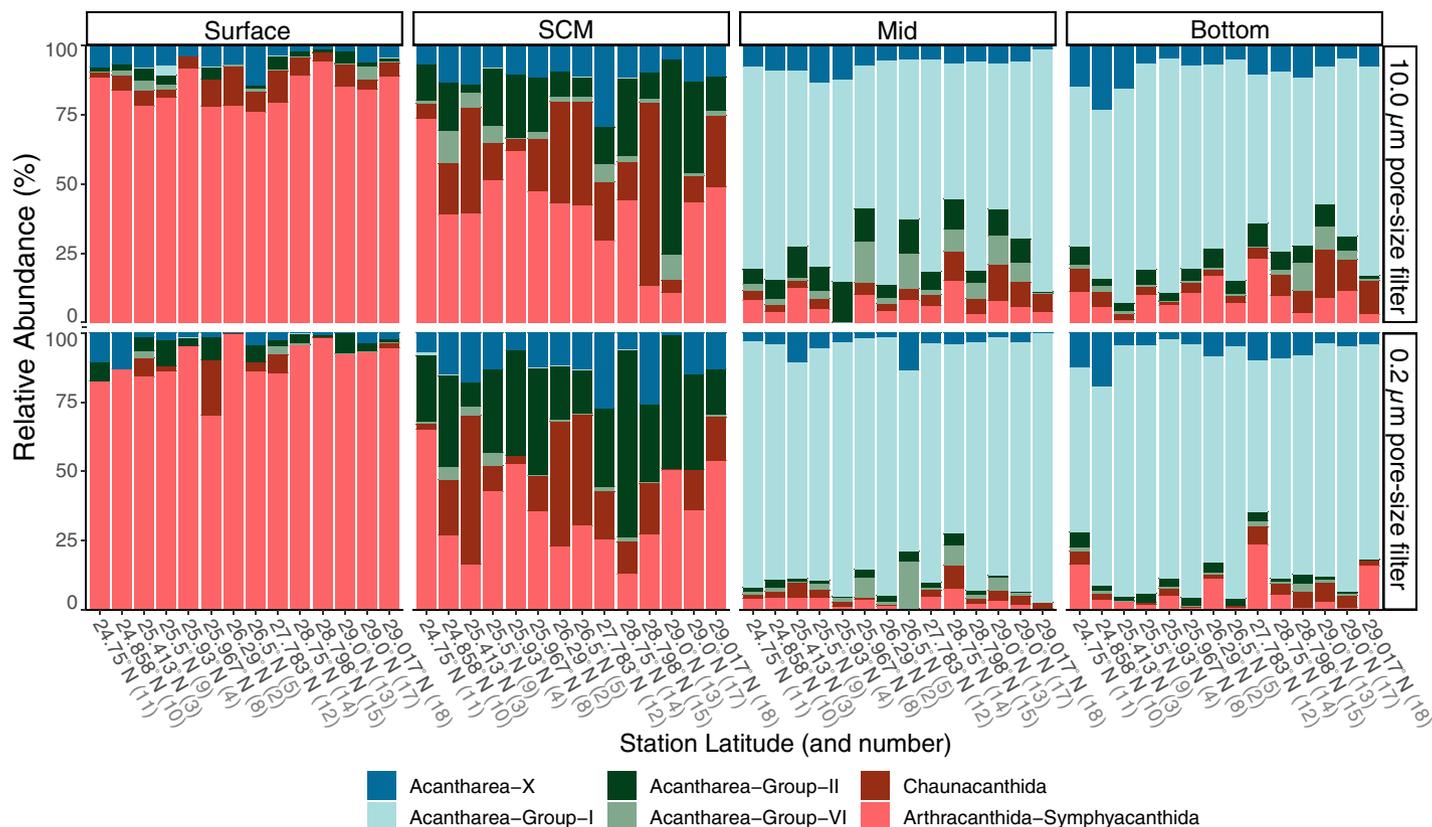

Fig. 3. Relative abundance of acantharian groups in size-fractionated samples from four depths in the western North Pacific. Each bar denotes the relative abundance of acantharian groups in replicate samples from a single station. Sampling stations are ordered on the x-axis from south to north and are labeled with their latitude and station number, corresponding to the sampling map in Fig. 1. The plot is faceted by sampling depth (columns) and filter pore size (rows). Colors indicate acantharian groups as classified with the PR^2 database. Acantharea-X (dark blue) represents sequences that were not classified past the class level (Acantharea).

the total number of protist sequences from each depth, (3) how the relative abundance of different acantharian clades varied by depth, and (4) if the acantharian contribution to total protist sequence numbers correlated to cell concentrations determined from imaging data. The data and code necessary to reproduce all statistical analyses are available on GitHub (https://github.com/maggimars/Acanth_ImageSeq),

including an interactive online document: https://maggimars.github.io/Acanth_ImageSeq/Acanth_ImageSeq_Analysis.html.

Results

Sequencing results

Overall, 31.5 million sequencing reads were generated for this study, with 34,631–421,992 sequencing reads per sample
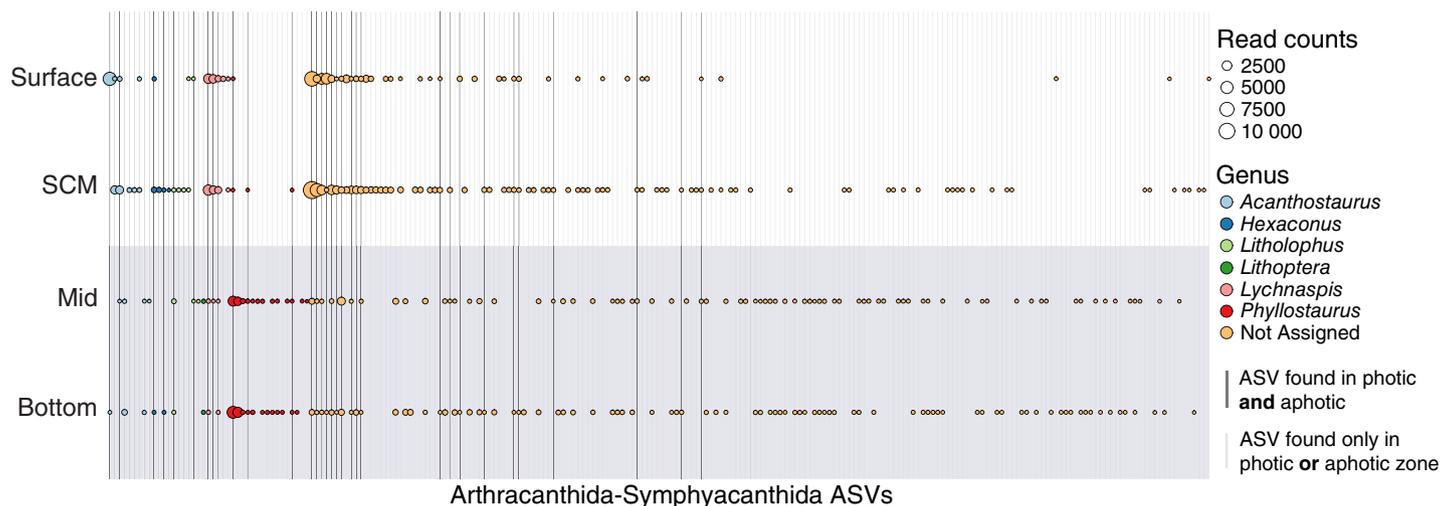

Fig. 4. Depth distribution of individual photosymbiotic acantharian sequence variants (Arthracanthida-Symphiacanthida). ASV abundance was aggregated for all samples collected at a given depth. Individual ASVs are plotted on the x-axis and depth layer is plotted on the y-axis. Point size represents ASV abundance (read counts) and point color corresponds to the genus each ASV was classified as belonging to with the PR^2 database (v4.11). Vertical gridlines are emphasized (in black) for all ASVs that were detected in samples collected from the surface or SCM (i.e., the photic zone) and samples collected from mid or bottom waters (i.e., aphotic zone). Thirty-two (14%) of the individual Arthracanthida-Symphycanthida ASVs were detected in samples from both the photic and aphotic zones.
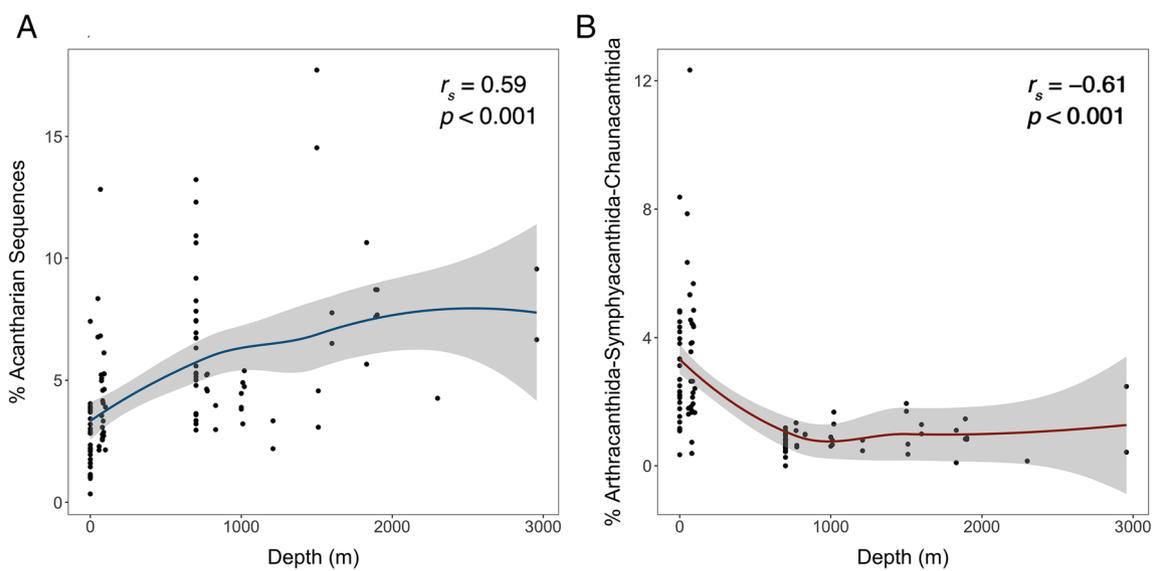

Fig. 5. Percentages of sequences deriving from all acantharians (**A**) and from Arthracanthida, Symphyacanthida, and Chaunacanthida acantharians (**B**) in samples collected on 10.0 μm pore-size filters. Sequence percentages refer to the proportion of sequences out of all denoised protist sequences for each of 108 samples. Curves were fit with local regression (loess) and 95% confidence intervals are shaded gray. Spearman correlation coefficients (r_s) and p values are included within plot panels. The percentages of all acantharian sequences were significantly positively correlated with depth, whereas the percentages of Arthracanthida, Symphyacanthida, and Chaunacanthida acantharians were significantly negatively correlated with depth.

(mean = 144,604). All raw sequence data are available from the NCBI Sequencing Read Archive, accession number PRJNA546472. Following denoising, 16.8 million sequences remained and 1.1 million ASVs were classified as Acantharea. We identified 1053 unique acantharian ASVs in our data set, out of a total of 22,656 unique ASVs.

In principal coordinates analyses (PCoA) of Aitchison distances between samples based on full protist community compositions, samples clustered by depth first, with clear separation of surface and SCM samples from mid and bottom water samples on the primary axis; SCM and surface samples further separated from each other on the secondary axis (Supporting Information Fig. S2A). When full protist communities were analyzed separately by depth, both surface and SCM samples segregated by filter pore size on primary axes and the mid-water samples segregated by filter pore size on

secondary axes (Supporting Information Fig. S3A), but these results were not found statistically significant with permutational analyses of variance. Notwithstanding, the clustering of full protist communities by filter pore size for surface, SCM, and mid-water samples suggests that size-fractionation was at least moderately successful. It remains likely, however, that some larger cells were broken or otherwise squeezed through the larger pore-sized filter to be captured on the lower filter, and that some smaller cells were stuck and retained on the larger pore-sized filter.

When only ASVs classified as Acantharea were included in PCoA based on Aitchison distances, samples also clustered first by depth, but the overall pattern was distinct from that seen when full protist communities were analyzed. Acantharian communities varied more in mid and bottom water samples than full protist communities did (Supporting Information
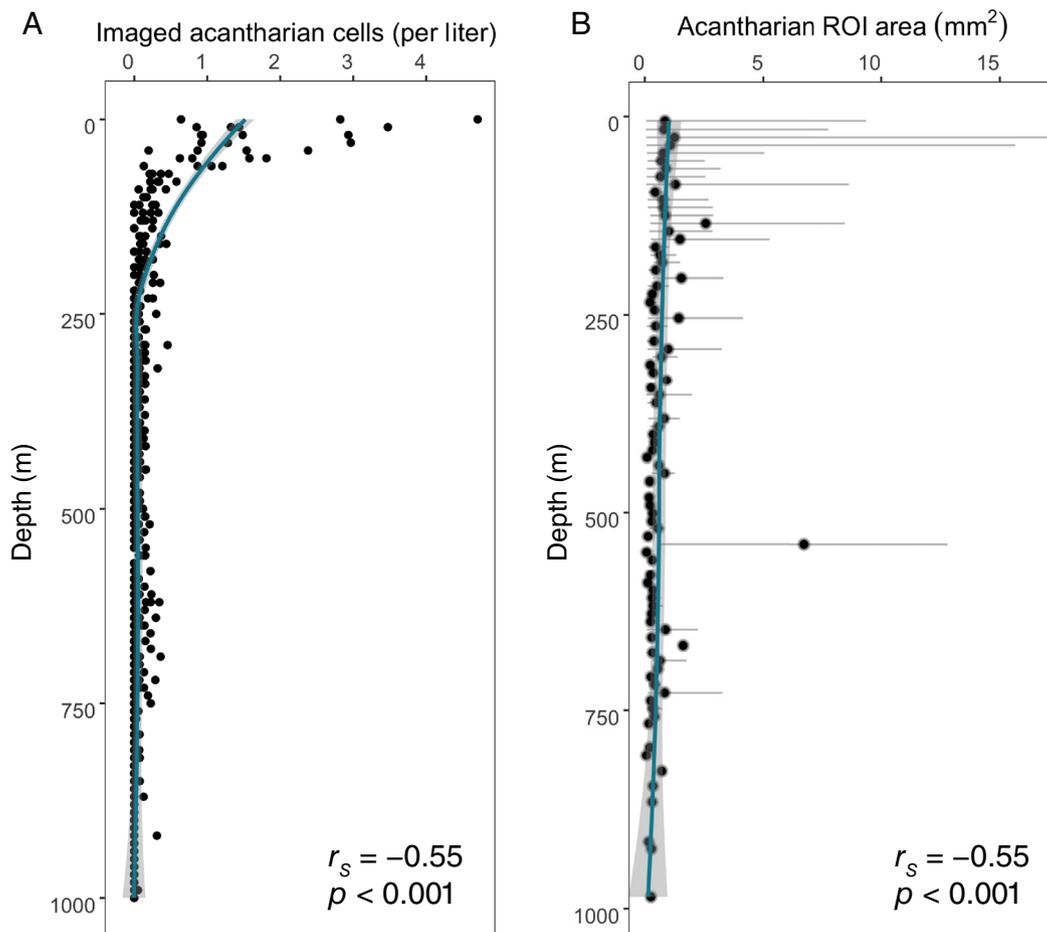

Fig. 6. Depth profiles for concentrations (**A**) and sizes (**B**) of imaged acantharians. Concentrations (**A**) were determined by dividing the number of cells observed in 10 m sections by the volume of water (in liters) imaged in that section for each of four stations ($n = 356$). The area of cropped acantharian ROIs (**B**) serves as a proxy for cell size; ROIs were cropped so that the edges of the rectangular photos aligned with the outward reaches of cellular extensions in each direction. The pixel dimensions of each ROI were converted to microns and the mean ROI area in 10 m bins for all stations are plotted as points, with whiskers denoting range (82 nonempty bins; 1235 cells). Curves were fit with local regression (loess) and 95% confidence intervals are shaded gray. Spearman correlation coefficients (r_s) and p values are included within plot panels. Both concentration and mean size of acantharian cells significantly decreased with depth.
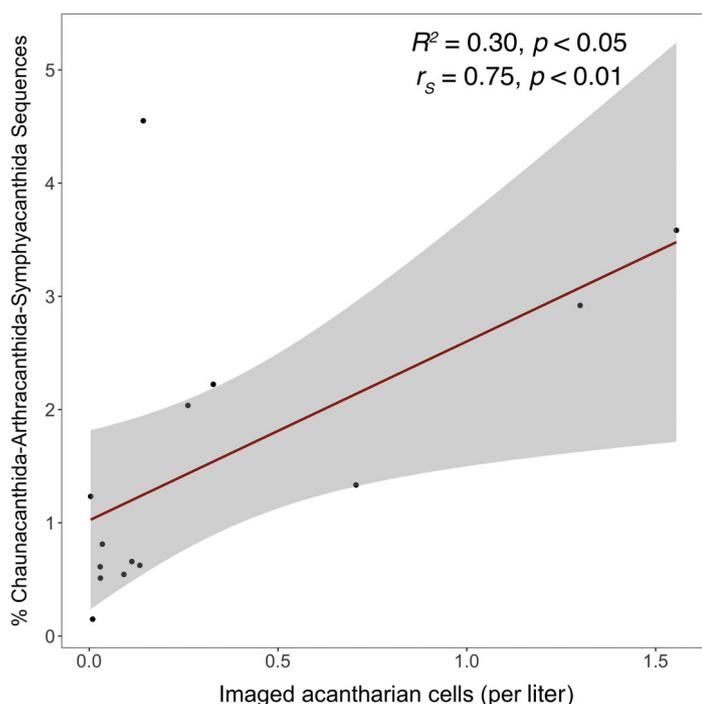
Fig. 7. Mean concentrations of imaged acantharian cells in surface, SCM, mid, and bottom depth layers and the percentage of sequences deriving from Chaunacanthida, Arthracanthida, and Symphyacanthida acantharians in corresponding samples. The trendline was fit with ordinary least squares regression and the R^2 and p value for the regression model (data are homoscedastic and residuals were normally distributed), as well as the spearman correlation coefficient (r_s) and p value (neither sequence percentages nor imaged cell concentrations were normally distributed), are included within the plot panel ($n = 14$). Percentage of sequences deriving from acantharians with known morphology (i.e., Chaunacanthida, Arthracanthida, and Symphyacanthida acantharians) significantly increases with the concentration of imaged acantharian cells.

Fig. S2B). Furthermore, while the full protist communities clustered separately by filter pore size in surface, SCM, and mid-water samples (Supporting Information Fig. S3A), this was not true for acantharian communities, which did not cluster by filter pore size at any depth (Supporting Information Fig. S3B).

At the surface, acantharians belonging to the photo-symbiotic orders Arthracanthida and Symphyacanthida (molecular clades E and F) made up almost the entire acantharian community in both large and small size-fraction samples at every station (Fig. 3). In the SCM, acantharians belonging to the largely nonsymbiotic, cyst-forming order Chaunacanthida (molecular clade C) additionally made up a large proportion of the acantharian community, as did acantharians belonging to the Acantharea-Group-II (molecular clade A) (Fig. 3), which can also form cysts (Decelle et al. 2013). In the mid and near-bottom water, the majority of the acantharian sequences derived from the Acantharea-Group-I (molecular clade I) (Fig. 3), which is one of several basal clades that

are defined entirely by sequences recovered from environmental samples and have no known morphology (Decelle et al. 2012*a*, 2013). While less abundant in samples from deep water, photosymbiotic acantharians (Arthracanthida-Symphyacanthida) were present in mid and bottom water samples at every station (Fig. 3) and 32 individual Arthracanthida-Symphyacanthida sequence variants (14%) were detected in samples from both the photic zone (i.e., surface or SCM) and the aphotic zone (i.e., mid or bottom water) (Fig. 4).

The relationship between depth and acantharian sequence abundance was evaluated by first calculating the percentage that acantharian sequences contributed to the full protist community in each of the 108 samples collected with a 10.0 μm pore-size filter (Fig. 5A). Because percentages were not normally distributed (Shapiro–Wilk test, $p < 0.05$), correlation between acantharian sequence percentage and sampling depth was tested for with the nonparametric Spearman rank correlation (r_s) test; acantharian sequence percentage was significantly positively correlated with depth ($r_s = 0.59$, $p < 0.001$). Since Chaunacanthida, Arthracanthida, and Symphyacanthida acantharians are known to possess the characteristic star-shape that was used to identify acantharians in images from this study, the percentages of sequences classified as Chaunacanthida, Arthracanthida, or Symphyacanthida were further considered separately (Fig. 5B). Percentages of sequences from these acantharians with known morphologies were significantly negatively correlated with depth ($r_s = -0.61$, $p < 0.001$)—opposite to the relationship when all acantharian sequences were analyzed together.

Imaging results

Overall, 1235 acantharian ROIs were identified and the vast majority of these were imaged near the sea surface (Fig. 6A). The concentration of imaged acantharian cells was significantly negatively correlated with depth ($r_s = -0.55$, $p < 0.001$), as was the mean size of observed acantharians ($r_s = -0.55$, $p < 0.001$). Acantharian cell size ranged widely in the surface waters and near the SCM, whereas the range was more constrained in deeper water (Fig. 6B). To directly evaluate how well imaging results reflected sequencing results, we averaged acantharian cell concentrations in each depth layer (surface: 0–50 m, SCM: 50–150 m, mid: 150–700 m, deep/bottom: > 700 m) at individual stations and directly compared these values to Chaunacanthida, Arthracanthida, and Symphyacanthida sequence percentages in samples from corresponding stations and depths (Fig. 7). Averaged cell concentrations significantly positively correlated with Chaunacanthida, Arthracanthida, and Symphyacanthida sequence abundance ($r_s = 0.75$, $p < 0.01$), following exclusion of two outlying data points with exceptionally high sequence abundance or imaged cell concentration (Fig. 7). Interestingly, many acantharians observed in surface waters had long pseudopodial extensions terminating in drop-shaped structures (Fig. 8). This morphology has not previously been observed
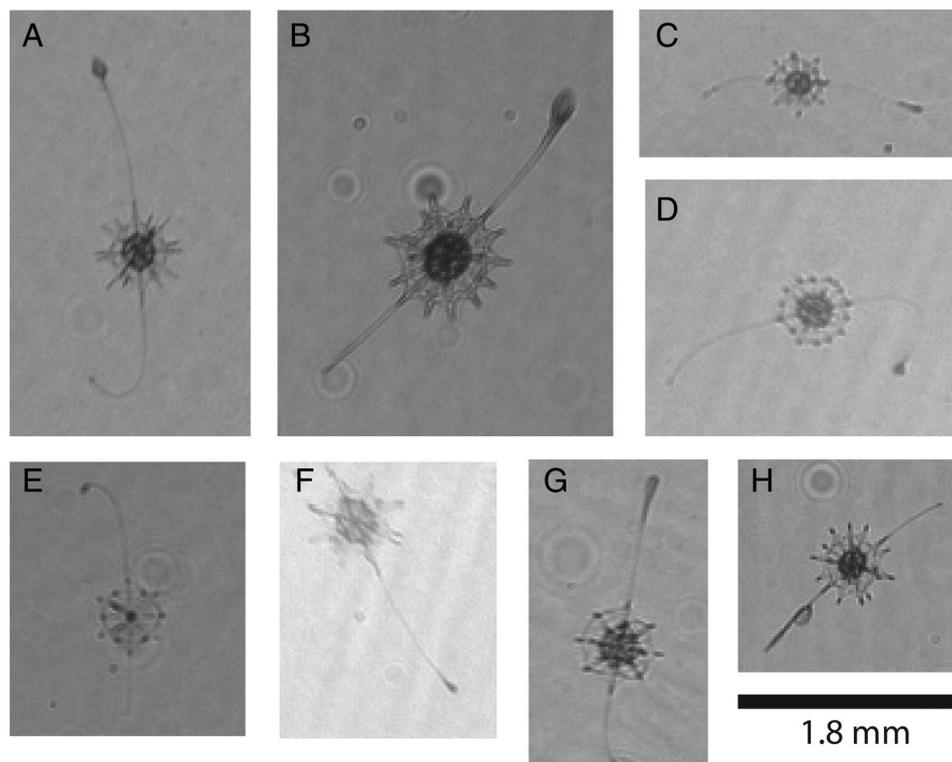
Fig. 8. In situ imaging reveals apparent acantharian predation behavior. Acantharians imaged in this study were observed with long pseudopodial extensions terminating in a drop-shaped structure. This behavior has not been described previously, potentially because the extensions are damaged in net-collected samples. Images were taken at 13.8 m, Sta. 15 (**A**); 16.4 m, Sta. 15 (**B**, **C**, **E**); 27.5 m, Sta. 15 (**D**); 31.2 m, Sta. 15 (**F**); 57.2 m, Sta. 17 (**G**); 13.8 m, Sta. 17 (**H**). Image aspect ratios are unaltered and the scale bar below panel (**H**) is accurate for all panels. Image orientations are likewise unchanged, with the top of images being toward the sea surface.

in acantharians, probably due to damage caused by plankton nets or other handling effects.

Discussion

Acantharians can be important contributors to carbon flux and primary production in different regions throughout the global ocean, but detailed studies on absolute abundance and fine-scale distribution have been hindered by specific acantharian traits, such as their fragile cell structures and skeletons that dissolve in common chemical fixatives. In addition, the smaller size of acantharians compared to other Rhizarians has precluded their full inclusion in quantitative in situ imaging surveys (Biard et al. 2016; Biard and Ohman 2020). As a result, recent advances in our understanding of acantharian biology and ecology have come primarily from molecular studies, but the relationship between results from molecular studies and other methods has not been evaluated. In this study, we took a paired approach and combined molecular survey methods with high-throughput, in situ imaging to better evaluate acantharian abundance and distribution. We found that vegetative acantharian cells were concentrated in the uppermost water column, but were

sporadically present throughout the water column, including at the deepest depths where images were taken (1000 m, Fig. 6A). The concentrations of acantharian cells determined from imaging correlated with the contribution of Arthracanthida, Symphyacanthida, and Chaunacanthida acantharians to all protist sequences recovered from the same depth and location (Fig. 5B). In contrast, the percentages of sequences from all acantharians, including those with unknown morphology, increased with depth (Fig. 5A). Together, these results can provide information about the distribution and abundance of different clades of acantharians, the morphology of undescribed environmental clades, and the life cycles of acantharians.

Acantharian abundance and distribution

In this study, we observed maximum acantharian abundances of 0.9–4.7 cells L^{-1} using an in situ camera system capable of imaging organisms with diameters greater than 250 μm (Fig. 6A). Maximum acantharian abundances were observed in the upper euphotic zone at each station: 0–10 m depth at Sta. 15 and 17, 20–30 m depth at Sta. 3, and 40–50 m depth at Sta. 10. These results are consistent with previous studies that

carefully preserved and counted acantharians collected by high-volume plankton pump and with Niskin bottles (Michaels 1991; Michaels et al. 1995). Michaels et al. (1995) observed near-surface acantharian maxima in the subtropical North Atlantic with maximum abundances ranging from 5.5 to 18 cells L^{-1} (mean 1.2 cells with > 100 μm diameter per liter in Niskin samples; mean 2.5 cells L^{-1} in pumped samples). Similarly, Michaels (1991) recorded 0.1–4 acantharian cells per liter (> 100 μm diameter) in the surface mixed layer of the eastern North Pacific Subtropical Gyre. Using high-throughput, in situ imaging, Biard and Ohman (2020) likewise found high acantharian concentrations near the sea surface in the California Current Ecosystem, although they identified acantharians only with diameter > 600 μm. Compared to other high-throughput imaging studies (Biard et al. 2016; Biard and Ohman 2020), the acantharian abundances we recorded are closer to the cell abundances reported when cells were counted by microscopy (Michaels 1991; Michaels et al. 1995). However, the cell abundances we measured are likely still an underestimate, since many acantharians are smaller than 250 μm (Michaels 1991; Michaels et al. 1995), and it would have been preferable to directly compare our imaging results with microscopy results from samples collected at the same and place. Nonetheless, the results from the high-throughput imaging in this study allow for a more quantitative estimate of acantharian abundance and vertical distribution in the western North Pacific than from analyzing sequencing data alone.

Basal environmental clades of Acantharea

The relative abundance of sequences classified as Chaunacanthida, Symphyacanthida, and Arthracanthida decreased as sampling depth increased (Fig. 5B), which correlated with the acantharian cell abundances determined from imaging data (Fig. 7). In contrast, the relative abundance of all sequences classified as Acantharea at the class level increased with depth (Fig. 5A). The additional acantharian sequences in communities from deeper water were primarily classified as Acantharea-Group-I (Fig. 3), which is basal to Chaunacanthida, Arthracanthida, and Symphyacanthida, and has no known morphology (Decelle et al. 2012a; Decelle and Not 2015). Similarly, the acantharian contribution to clone libraries from coastal waters near California increased with depth (Schnetzer et al. 2011) and environmental sequences from basal acantharian clades have been recovered from deep waters throughout the global ocean (López-García et al. 2001; Edgcomb et al. 2002; Countway et al. 2007; Not et al. 2007; Terrado et al. 2009; Gilg et al. 2010; Quaiser et al. 2011; Decelle et al. 2013). Here, the discrepancy between the depth-related increase in sequence abundance for Acantharea-Group-I and the coinciding decline in cells imaged with characteristic acantharian morphologies may provide new evidence regarding the morphology of basal environmental acantharian clades.

The acantharian skeleton is a central feature to their morphological classification; the most recently diverged clades (Arthacanthida and Symphyacanthida) have spicules of varying lengths—some with elaborate protrusions—that are fused in a robust central junction, whereas earlier diverging clades (e.g., Chaunacanthida, Acantharea-Group-II) have simpler spicules of equal length that either cross the central region of the cell or form loosely fused central junctions (Decelle et al. 2012a). This evolutionary trajectory—from less to more developed skeletons—suggests that the earliest diverging acantharian clades (e.g., basal environmental clade I) may have only rudimentary skeletal structures, or may lack the quintessential acantharian skeleton altogether (Decelle et al. 2012a). The decreased observance of recognizable acantharian cells with depth coinciding with an increased abundance of sequences from clade I acantharians suggests that they may, indeed, lack traditionally recognized acantharian morphologies. Alternatively, clade I acantharians may simply be too small to be imaged with the ISIIS small-imager used in this study. Ultimately, the morphology of the most basal environmental acantharian clades can only be definitively resolved with single-cell sequencing of deep-sea isolates coupled with microscopy (Sieracki et al. 2019). However, our results demonstrate that small cells lacking symmetrical strontium sulfate skeletons should be considered for sequencing in studies seeking to determine the morphology of the earliest diverging acantharian clades.

Acantharian life cycles

Knowledge regarding acantharian life cycles remains relatively limited because a full acantharian life cycle has not yet been directly observed in laboratory conditions and acantharians are not currently in culture (Decelle et al. 2012b). Like other rhizarians—including radiolaria (Anderson 1983; Kimoto et al. 2011) and foraminifera (Bé et al. 1983)—acantharians release small (2–3 μm), flagellated swarmer cells that are assumed to be reproductive gametes (Decelle et al. 2012b). While syngamy of acantharian swarmers has not been observed, swarmer release from both acantharian cysts and vegetative cells has been witnessed in laboratory settings (Decelle et al. 2012b, 2013). So far, cyst formation has only been observed for earlier diverging acantharian lineages and has not been seen among Arthracanthida or Symphyacanthida acantharians. Acantharians that form cysts shed most of their spicules before cyst formation, suggesting that acantharians in later diverging clades, with more robust and elaborate skeletons, cannot form cysts because of the fixed central junctions in their skeletons. In addition, cysts recovered from sediment traps have only ever belonged to earlier diverging clades based on phylogenetic analysis—but not environmental clade I (Decelle et al. 2013). As a result, current hypotheses propose that acantharians in earlier diverging clades, including Chaunacanthida and Acantharea-Group-II acantharians, form cysts as a means for ballast, allowing them to sink into deep water where they release swarmer cells, whereas the later diverging Arthracanthida and Symphyacanthida acantharians complete their life cycle in the photic zone, since they

cannot form cysts and need to acquire photosymbionts at the start of each generation (Martin et al. 2010; Decelle et al. 2013).

Imaging results demonstrating decreased acantharian abundance and size below the surface mixed layer (Fig. 6) are consistent with hypotheses regarding acantharian life cycles, specifically that many acantharians sink to release swarmers and that juveniles grow in size as they make their way toward the surface. Adult vegetative cells, along with cysts, have high potential sinking rates due to the specific gravity of biomineralized strontium sulfate (Michaels et al. 1995), which, combined with the fact that both vegetative cells and cysts dissociate after releasing swarmers (Decelle et al. 2012*b*, 2013), makes them less likely to be caught on camera. A large number of swarmers released at depth would potentially produce many small juvenile cells that gradually increase in size as they slowly ascend. These smaller, more abundant juveniles would be more likely to be imaged than the rarer, fast-sinking adults, thus providing one explanation as to why smaller cells were imaged more often than large cells in deep water (Fig. 6B). Alternatively, reduced cell-size (mean and range) at depth could reflect decreased nutritional resources available in deeper waters or constitutively smaller-sized species being more common below the surface mixed layer (Robinson et al. 2010). However, deep-sea organisms can also often exhibit gigantism (McClain et al. 2006), and very large protists, including radiolaria and phaeodaria, are found in the mesopelagic zone (Boltovskoy et al. 2010; Biard et al. 2016; Stukel et al. 2018). In this case, the sporadic presence of large acantharian cells in deep water is evidence that large cells do sink into deep water or that acantharians can grow to large sizes at depth (Fig. 6B).

By combining metabarcoding of size-fractionated samples with imaging, further insight into acantharian life cycles can be gained. In principle, vegetative cells and cysts should have been retained on the larger pore-sized upper filter and swarmer cells should have passed through the upper filter and been retained on the smaller pore-sized lower filter. A disparity in the contribution of one clade to sequences in the two size-fractions could, therefore, indicate that vegetative cells or reproductive cells from that clade are more or less abundant at a particular depth. This is especially true since a single acantharian vegetative cell or cyst can release thousands of individual swarmer cells, which would, therefore, contribute many copies of the 18S rRNA gene sequence. Such size fractionation can never be perfect—and it may be especially problematic with delicate cells like acantharians—but principal coordinate analysis (PCoA) of Aitchison distances between full protist communities demonstrated segregation by filter type (Supporting Information Fig. S3A), thus suggesting size-fractionation was moderately successful. In contrast, PCoA for acantharian communities in the same samples did not show any segregation by filter type (Supporting Information Fig. S3B), thus providing evidence that swarmers and vegetative cells or cysts could coexist at the depths sampled. Given that Chaunacanthida acantharians are among those that form cysts and are believed to sink before releasing

swarmers, Chaunacanthida would be expected to be more abundant than noncysting Arthracanthida and Symphyacanthida in both size fractions at depth. Interestingly, Arthracanthida and Symphyacanthida sequences were recovered from both large and small size-fraction samples from mid and near-bottom water at every sampling station and had similar relative abundances to Chaunacanthida sequences (Fig. 3). Furthermore, individual Arthracanthida and Symphycanthida exact sequence variants were found in samples from the euphotic zone and from deeper waters (Fig. 4).

The lack of differentiation between sequence abundances for Arthracanthida-Symphyacanthida and Chaunacanthida acantharians in deep water, together with the recovery of identical Arthracanthida and Symphyacanthida ASVs in surface and deep-water samples, suggests that later diverging acantharian clades may not complete their entire life cycle in photic zone. An alternative hypothesis might be that Arthracanthida and Symphyacanthida acantharians also sink into deep water to reproduce, but do so as vegetative cells—aided by their robust skeletons and fine buoyancy control (Febvre and Febvre-Chevalier 2001)—rather than in the form of cysts (Michaels et al. 1995). Similarly, sequences from a polycystine radiolarian that directly releases swarmers from vegetative cells have also been recovered from the picoplankton size-fraction of samples collected from deep water (Not et al. 2007; Kimoto et al. 2011), suggesting that releasing swarmers at depth may be widespread among rhizarians, regardless of cyst formation. Of course, it cannot be ruled out that the DNA recovered from deep waters could be extracellular or derive from detrital matter and future work on this topic would benefit from RNA sequencing. However, the migration of vegetative cells into deeper water to reproduce is supported by observations of large vegetative acantharian cells at depth (Fig. 6B, Biard and Ohman 2020).

Acantharian behavior revealed by in situ imaging

Being notoriously delicate and sticky, acantharians are often broken or clumped when collected by plankton net. As a result, their fine structure is usually damaged even when they do survive collection, which can preclude behavioral observations. In situ imaging is especially useful in such cases, as it allows for the observation of natural orientation and behaviors that could not otherwise be seen. Acantharians are known to consume other planktonic organisms: microscopy with SCUBA collected acantharians revealed ciliates, diatoms, and dinoflagellates as acantharian prey items within acantharian vacuoles (Swanberg and Caron 1991) and results from 18S sequence analysis of single acantharians included copepod, diatom, and dinoflagellate sequences (Mars Brisbin et al. 2018). Actual predatory strategies of acantharians are currently unknown, but other rhizarians have been observed deploying diverse predatory strategies: some phaeodarians use protoplasmic webs between skeletal projections to trap prey and pseudopodial "tentacles" that actively grab prey

(Nakamura et al. 2018), several polycystine radiolarians extend extra-long feeding pseudopods that catch prey with a "terminal cone" (Matsuoka 2007), and other polycystine radiolarians envelope prey snagged in pseudopodial extensions in vacuoles to transport prey toward the cell center (Anderson 1978). In this study, we repeatedly observed acantharians near the sea surface that had long pseudopodial extensions terminating in drop-shaped structures. This morphology/behavior has not been previously reported for acantharians and we hypothesize that the extensions are related to a predatory strategy. The drop-shaped structures may represent a fishing apparatus, similar to the terminal cone in polycystine radiolarians (Matsuoka 2007), that allows acantharians to lure and capture prey. Alternatively, the drop-shaped structures may be already-captured prey within vacuoles (Anderson 1978); in Fig. 8H, the drop-structure seems to be moving toward the cell center along the pseudopodial extension. We did not observe prey items attached to or within the acantharian drop-structures, but it unlikely that acantharian prey are large enough to be well resolved in our images. However, it remains possible that these drop-shaped structures may be involved in processes other than predation (e.g., reproduction, buoyancy, or locomotion).

Conclusions

The high-throughput imaging used in this study showed that acantharians are abundant in the surface waters of the western North Pacific (East China Sea) and are found at comparable concentrations as have been reported in the eastern North Pacific and the North Atlantic where cells were manually counted with microscopy. Similar to previous studies, vegetative acantharian cells were concentrated very close to the sea surface and decreased in abundance with depth, but were still sometimes observed at depths approaching 1000 m. Imaging data correlated with sequence abundances from acantharian clades with known and easily recognizable morphologies, but were in contrast to sequence abundances from acantharian environmental clade I, which has unknown morphology. This discrepancy suggests that basal environmental clades, such as clade I, may have morphologies distinct from other acantharians and may lack characteristic star-shaped strontium sulfate skeletons. The size distribution of imaged acantharians is consistent with current hypotheses about acantharian life cycles: size decreases with depth, supporting the idea that acantharians reproduce at depth by releasing small swarmer cells, followed by the ascension and growth of juveniles into surface waters. However, the similar relative abundance of different acantharian clades in small and large size fractions at depth suggests that later diverging clades (i.e., Arthracanthida and Symphyacanthida) may also reproduce at depth, which is counter to previous hypotheses. By pairing high-throughput sequencing with high-throughput, in situ imaging, this study advances our understanding of acantharian biology but also highlights how much is still unknown. Future studies will benefit from the annotated images produced

in this study, but should consider further pairing imaging with RNA sequencing or single-cell genomics. Accurate automatic classification will eventually allow for larger studies of acantharian abundance and distribution, including expanded geographic and temporal scales, and thus a deeper understanding of acantharian contributions to biogeochemical processes in the ocean.

References

Anderson, O. R. 1978. Light and electron microscopic observations of feeding behavior, nutrition, and reproduction in laboratory cultures of *Thalassicolla nucleata*. Tissue Cell **10**: 401–412. doi:10.1016/S0040-8166(16)30336-6

Anderson, O. R. 1983. Radiolaria. Springer-Verlag.

Bé, A. W. H., O. R. Anderson, W. W. Faber, and D. A. Caron. 1983. Sequence of morphological and cytoplasmic changes during gametogenesis in the planktonic foraminifer *Globigerinoides sacculifer* (Brady). Micropaleontology **29**: 310–325. doi:10.2307/1485737

Beers, J. R., and G. L. Stewart. 1970. The preservation of acantharians in fixed plankton samples. Limnol. Oceanogr. **15**: 825–827. doi:10.4319/lo.1970.15.5.0825

Belcher, A., C. Manno, S. Thorpe, and G. Tarling. 2018. Acantharian cysts: High flux occurrence in the bathypelagic zone of the Scotia Sea, Southern Ocean. Mar. Biol. **165**: 117. doi:10.1007/s00227-018-3376-1

Bernstein, R. E., P. R. Betzer, R. A. Feely, R. H. Byrne, M. F. Lamb, and A. F. Michaels. 1987. Acantharian fluxes and strontium to chlorinity ratios in the north pacific ocean. Science **237**: 1490–1494. doi:10.1126/science.237.4821.1490

Biard, T., and others. 2016. In situ imaging reveals the biomass of giant protists in the global ocean. Nature **532**: 504–507.

Biard, T., E. Bigeard, S. Audic, J. Poulain, A. Gutierrez-Rodriguez, S. Pesant, L. Stemmann, and F. Not. 2017. Biogeography and diversity of Collodaria (Radiolaria) in the global ocean. ISME J. **11**: 1331–1344. doi:10.1038/ismej.2017.12

Biard, T., and M. D. Ohman. 2020. Vertical niche definition of test-bearing protists (Rhizaria) into the twilight zone revealed by in situ imaging. Limnol. Oceanogr. **10**: 401.

Bokulich, N. A., and others. 2018. Optimizing taxonomic classification of marker-gene amplicon sequences with QIIME 2's q2-feature-classifier plugin. Microbiome **6**: 90. doi:10.1186/s40168-018-0470-z

Boltovskoy, D., S. A. Kling, K. Takahashi, and K. Bjørklund. 2010. World atlas of distribution of recent polycystina (Radiolaria). **13**.

Bolyen, E., and others. 2019. Reproducible, interactive, scalable and extensible microbiome data science using QIIME 2. Nat. Biotechnol. **37**: 852–857. doi:10.1038/s41587-019-0209-9

Callahan, B. J., P. J. McMurdie, M. J. Rosen, A. W. Han, A. J. A. Johnson, and S. P. Holmes. 2016. DADA2: High-resolution sample inference from Illumina amplicon data. Nat. Methods **13**: 581–583. doi:10.1038/nmeth.3869

Countway, P. D., D. A. Caron, R. J. Gast, and P. Savai. 2007. Comparison of protistan diversity in deep (2500 m) vs euphotic zone assemblages in the Sargasso Sea and Gulf Stream (N. Atlantic). Environ. Microbiol. **9**: 1219–1232. doi:10.1111/j.1462-2920.2007.01243.x

Countway, P. D., P. D. Vigil, A. Schnetzer, S. D. Moorthi, and D. A. Caron. 2010. Seasonal analysis of protistan community structure and diversity at the USC Microbial Observatory (San Pedro Channel, North Pacific Ocean). Limnol. Oceanogr. **55**: 2381–2396. doi:10.4319/lo.2010.55.6.2381

Cowen, R. K., and C. M. Guigand. 2008. In situ ichthyoplankton imaging system (ISIIS): system design and preliminary results. Limnol. Oceanogr. Methods. **6**: 126–132.

de Vargas, C., and others. 2015. Ocean plankton. Eukaryotic plankton diversity in the sunlit ocean. Science **348**: 1261605. doi:10.1126/science.1261605

Decelle, J., N. Suzuki, F. Mahé, C. de Vargas, and F. Not. 2012*a*. Molecular phylogeny and morphological evolution of the Acantharia (Radiolaria). Protist **163**: 435–450. doi:10.1016/j.protis.2011.10.002

Decelle, J., and others. 2012*b*. An original mode of symbiosis in open ocean plankton. Proc. Natl. Acad. Sci. USA **109**: 18000–18005. doi:10.1073/pnas.1212303109

Decelle, J., and others. 2013. Diversity, ecology and biogeochemistry of cyst-forming acantharia (radiolaria) in the oceans. PLoS One **8**: e53598. doi:10.1371/journal.pone.0053598

Decelle, J., S. Romac, E. Sasaki, F. Not, and F. Mahé. 2014. Intracellular diversity of the V4 and V9 regions of the 18S rRNA in marine protists (radiolarians) assessed by high-throughput sequencing. PLoS One **9**: e104297. doi:10.1371/journal.pone.0104297

Decelle, J., and F. Not. 2015. Acantharia. eLS **59**: 1–10. doi:10.1002/9780470015902.a0002102.pub2

Dennett, M. R., D. A. Caron, A. F. Michaels, S. M. Gallager, and C. S. Davis. 2002. Video plankton recorder reveals high abundances of colonial Radiolaria in surface waters of the central North Pacific. J. Plankton Res. **24**: 797–805. doi:10.1093/plankt/24.8.797

Edgcomb, V. P., D. T. Kysela, A. Teske, A. de Vera Gomez, and M. L. Sogin. 2002. Benthic eukaryotic diversity in the Guaymas Basin hydrothermal vent environment. Proc. Natl. Acad. Sci. USA **99**: 7658–7662. doi:10.1073/pnas.062186399

Febvre, J., and C. Febvre-Chevalier. 2001. Acantharia. eLS **32**: 211. doi:10.1038/npg.els.0002102

Fontanez, K. M., J. M. Eppley, T. J. Samo, D. M. Karl, and E. F. DeLong. 2015. Microbial community structure and function on sinking particles in the North Pacific Subtropical Gyre. Front. Microbiol. **6**: 469. doi:10.3389/fmicb.2015.00469

Gaskell, D. E., M. D. Ohman, and P. M. Hull. 2019. Zooglider-based measurements of planktonic foraminifera in the California Current System. J. Foraminifer. Res. **49**: 390–404. doi:10.2113/gsjfr.49.4.390

Gilg, I. C., L. A. Amaral-Zettler, P. D. Countway, S. Moorthi, A. Schnetzer, and D. A. Caron. 2010. Phylogenetic affiliations of mesopelagic acantharia and acantharian-like environmental 18S rRNA genes off the southern California coast. Protist **161**: 197–211. doi:10.1016/j.protis.2009.09.002

Gloor, G. B., J. M. Macklaim, V. Pawlowsky-Glahn, and J. J. Egozcue. 2017. Microbiome datasets are compositional: And this is not optional. Front. Microbiol. **8**: 2224. doi:10.3389/fmicb.2017.02224

Gong, W., and A. Marchetti. 2019. Estimation of 18S gene copy number in marine eukaryotic plankton using a next-generation sequencing approach. Front. Mar. Sci. **6**: 219. doi:10.3389/fmars.2019.00219

Greer, A. T., R. K. Cowen, C. M. Guigand, M. A. McManus, J. C. Sevadjian, and A. H. V. Timmerman. 2013. Relationships between phytoplankton thin layers and the fine-scale vertical distributions of two trophic levels of zooplankton. J. Plankton Res. **35**: 939–956. doi:10.1093/plankt/fbt056

Grossmann, M. M., S. M. Gallager, and S. Mitarai. 2015. Continuous monitoring of near-bottom mesoplankton communities in the East China Sea during a series of typhoons. J. Oceanogr. **71**: 115–124. doi:10.1007/s10872-014-0268-y

Guillou, L., and others. 2013. The Protist Ribosomal Reference database (PR2): A catalog of unicellular eukaryote small sub-unit rRNA sequences with curated taxonomy. Nucleic Acids Res. **41**: D597–D604. doi:10.1093/nar/gks1160

Gutierrez-Rodriguez, A., M. R. Stukel, A. Lopes Dos Santos, T. Biard, R. Scharek, D. Vaulot, M. R. Landry, and F. Not. 2019. High contribution of Rhizaria (Radiolaria) to vertical export in the California Current Ecosystem revealed by DNA metabarcoding. ISME J. **13**: 964–976. doi:10.1038/s41396-018-0322-7

Hu, S. K., P. E. Connell, L. Y. Mesrop, and D. A. Caron. 2018. A hard day's night: Diel shifts in microbial eukaryotic activity in the North Pacific Subtropical Gyre. Front. Mar. Sci. **5**: 351. doi:10.3389/fmars.2018.00351

Kimoto, K., T. Yuasa, and O. Takahashi. 2011. Molecular identification of reproductive cells released from *Cypassis irregularis* Nigrini (Radiolaria). Environ. Microbiol. Rep. **3**: 86–90. doi:10.1111/j.1758-2229.2010.00191.x

Lombard, F., and others. 2019. Globally consistent quantitative observations of planktonic ecosystems. Front. Mar. Sci. **6**: 1705. doi:10.3389/fmars.2019.00196

López-García, P., F. Rodríguez-Valera, C. Pedrós-Alió, and D. Moreira. 2001. Unexpected diversity of small eukaryotes in deep-sea Antarctic plankton. Nature **409**: 603–607. doi:10.1038/35054537

Mars Brisbin, M., L. Y. Mesrop, M. M. Grossmann, and S. Mitarai. 2018. Intra-host symbiont diversity and extended symbiont maintenance in photosymbiotic Acantharea (clade F). Front. Microbiol. **9**: 1998. doi:10.3389/fmicb.2018.01998

Martin, P., J. T. Allen, M. J. Cooper, D. G. Johns, R. S. Lampitt, R. Sanders, and D. A. H. Teagle. 2010. Sedimentation of acantharian cysts in the Iceland Basin: Strontium as a ballast for deep ocean particle flux, and implications for acantharian

reproductive strategies. Limnol. Oceanogr. **55**: 604–614. doi:10.4319/lo.2010.55.2.0604

Matsuoka, A. 2007. Living radiolarian feeding mechanisms: New light on past marine ecosystems. Swiss J. Geosci. **100**: 273–279. doi:10.1007/s00015-007-1228-y

McClain, C. R., A. G. Boyer, and G. Rosenberg. 2006. The Island rule and the evolution of body size in the deep sea. J. Biogeogr. **33**: 1578–1584. doi:10.1111/j.1365-2699.2006.01545.x

McMurdie, P. J., and S. Holmes. 2013. Phyloseq: An R package for reproducible interactive analysis and graphics of micro-biome census data. PLoS One **8**: e61217. doi:10.1371/journal.pone.0061217

Michaels, A. F. 1988. Vertical distribution and abundance of Acantharia and their symbionts. Mar. Biol. **97**: 559–569. doi:10.1007/BF00391052

Michaels, A. F. 1991. Acantharian abundance and symbiont productivity at the VERTEX seasonal station. J. Plankton Res. **13**: 399–418. doi:10.1093/plankt/13.2.399

Michaels, A. F., D. A. Caron, N. R. Swanberg, F. A. Howse, and C. M. Michaels. 1995. Planktonic sarcodines (Acantharia, Radiolaria, Foraminifera) in surface waters near Bermuda: Abundance, biomass and vertical flux. J. Plankton Res. **17**: 131–163. doi:10.1093/plankt/17.1.131

Nakamura, Y., R. Somiya, M. Kanda, A. Yamaguchi, A. Tuji, and R. S. Hori. 2018. *Gazelletta kashiwaensis* sp. nov. (Medusettidae, Phaeodaria, Cercozoa), its morphology, phylogeny, distribution, and feeding behavior. J. Eukaryot. Microbiol. **65**: 923–927. doi:10.1111/jeu.12516

Not, F., R. Gausling, F. Azam, J. F. Heidelberg, and A. Z. Worden. 2007. Vertical distribution of picoeukaryotic diversity in the Sargasso Sea. Environ. Microbiol. **9**: 1233–1252. doi:10.1111/j.1462-2920.2007.01247.x

Orenstein, E. C., O. Beijbom, E. E. Peacock, and H. M. Sosik. 2015. WHOI-plankton—a large scale fine grained visual recognition benchmark dataset for plankton classification. arXiv [cs.CV]. arXiv:1510.00745v1.

Peacock, E. E., R. J. Olson, and H. M. Sosik. 2014. Parasitic infection of the diatom *Guinardia delicatula*, a recurrent and ecologically important phenomenon on the New England shelf. Mar. Ecol. Prog. Ser. **503**: 1–10. doi:10.3354/meps10784

Pernice, M. C., C. R. Giner, R. Logares, J. Perera-Bel, S. G. Acinas, C. M. Duarte, J. M. Gasol, and R. Massana. 2016. Large variability of bathypelagic microbial eukaryotic communities across the world's oceans. ISME J. **10**: 945–958. doi:10.1038/ismej.2015.170

Quaiser, A., Y. Zivanovic, D. Moreira, and P. López-García. 2011. Comparative metagenomics of bathypelagic plankton and bottom sediment from the sea of Marmara. ISME J. **5**: 285–304. doi:10.1038/ismej.2010.113

R Core Team. 2018. R: A language and environment for statistical computing.

Robinson, C., and others. 2010. Mesopelagic zone ecology and biogeochemistry – a synthesis. Deep-Sea Res. Part II Top. Stud. Oceanogr. **57**: 1504–1518. doi:10.1016/j.dsr2.2010.02.018

Schnetzer, A., S. D. Moorthi, P. D. Countway, R. J. Gast, I. C. Gilg, and D. A. Caron. 2011. Depth matters: Microbial eukaryote diversity and community structure in the eastern North Pacific revealed through environmental gene libraries. Deep-Sea Res. Part I Oceanogr. Res. Pap. **58**: 16–26. doi:10.1016/j.dsr.2010.10.003

Sieracki, M. E., and others. 2010. Optical plankton imaging and analysis systems for ocean observation. Proceedings of ocean Obs. **9**: 21–25.

Sieracki, M. E., and others. 2019. Single cell genomics yields a wide diversity of small planktonic protists across major ocean ecosystems. Scientific reports. **9**: 1–11. doi:10.1038/s41598-019-42487-1

Stoeck, T., D. Bass, M. Nebel, R. Christen, M. D. M. Jones, H.-W. Breiner, and T. A. Richards. 2010. Multiple marker parallel tag environmental DNA sequencing reveals a highly complex eukaryotic community in marine anoxic water. Mol. Ecol. **19**: 21–31. doi:10.1111/j.1365-294X.2009.04480.x

Stukel, M. R., T. Biard, J. Krause, and M. D. Ohman. 2018. Large Phaeodaria in the twilight zone: Their role in the carbon cycle. Limnology and Oceanography. **63**: 2579–2594. doi:10.1002/lno.10961

Swanberg, N. R., and D. A. Caron. 1991. Patterns of sarcodine feeding in epipelagic oceanic plankton. J. Plankton Res. **13**: 287–312. doi:10.1093/plankt/13.2.287

Terrado, R., W. F. Vincent, and C. Lovejoy. 2009. Mesopelagic protists: diversity and succession in a coastal Arctic ecosystem. Aquatic microbial ecology. **56**: 26–39. doi:10.3354/ame01327

Torti, A., M. A. Lever, and B. B. Jørgensen. 2015. Origin, dynamics, and implications of extracellular DNA pools in marine sediments. Mar. Genomics **24**: 185–196. doi:10.1016/j.margen.2015.08.007

Conflict of Interest

None declared.